

# Modulation instability in high-order coupled nonlinear Schrödinger equations with saturable nonlinearities

Erivelton O. Alves, Wesley B. Cardoso, and Ardiley T. Avelar  
*Instituto de Física, Universidade Federal de Goiás, 74.001-970, Goiânia, Goiás, Brazil*

The influence of a saturable nonlinearity on the modulation instability in oppositely directed coupler in the presence of high-order effects is investigated. By using the standard linear stability analysis, we obtain the instability gain that exhibits a significant change in the bands of instability due to the effects of a saturable nonlinearity. We also show that even in the presence of saturation there is no change in instability gain when we compare the results obtained for both channels not influenced by self-steepening effect or for both channels influenced by self-steepening effect but opposite in sign. Regarding the Raman effect, there is reflection symmetry (asymmetry) to the gain at zero perturbation frequency when the values of the Raman coefficients in each directional coupler are equal and with same (opposite) sign. For the anomalous group velocity dispersion regime we observe that the growth of the saturation parameter is followed by an increase in the null gain region near  $\Omega = 0$ , enlarging the separation of the instability bands close to this point. Finally, we show that an efficient control of the modulation instability can be realized by adjusting self-steepening effect and intrapulse Raman scattering, even in the presence of a saturable nonlinearity.

PACS numbers: 05.45.-a, 42.65.Dr, 42.65.Sf, 42.65.Wi

## I. INTRODUCTION

Modulational instability (MI) is a ubiquitous phenomenon associated with an exponential growth of the amplitude of a weak perturbed continuous wave in certain conditions during its propagation under the interplay between diffraction (in spatial domain) or dispersion (in temporal domain) and nonlinearity. This phenomenon has been observed and/or predicted in various nonlinear systems such as plasma waves [1–4], hydromagnetic waves [5], optical fibers [6, 7], dust-acoustic and dust-ion-acoustic waves [8], noninstantaneous nonlinear media [9, 10], Bose-Einstein condensates [11–14], liquid crystals [15], ocean waves [16, 17], and so on. In nonlinear optics, MI has been studied in lossy fibers [18], fiber gratings [19], for incoherent light [9], and second harmonic generation [20]; and with different type of the nonlinear response such as integrating [21], nonlocal [22], quadratic [23], cubic-quintic [24], varying [25], and saturable one [26, 27], and so on. In addition, a train of solitons can emerge from a system that presents MI allowing us to generate subpicosecond solitonlike optical pulses, such as those presented in [28, 29]. A historical review on this subject can be found in [30].

Coupled systems is also a good candidate for the investigation of MI and several studies have been proposed in this type of systems, such as the parametric amplification and MI in dispersive nonlinear directional couplers made from two (or more) coupled guiding channels (e.g., two physically distinct waveguides or two polarization modes) exhibiting an intensity-dependent refractive index with relaxing nonlinearity [31], wide beam stabilities and instabilities in one dimensional arrays of Kerr-nonlinear channel waveguides [32], MI in two-core optical fibers incorporating the ef-

fects of coupling-coefficient dispersion [33], MI in birefringent two-core optical fibers [34], the role of the coupling-induced group velocity dispersion on the MI in a silicon-on-insulator directional coupler [35], MI in a twin-core fiber with the effect of saturable nonlinear response and coupling coefficient dispersion [36], the investigation of the dynamic properties of a nonlinear directional coupler made of Kerr materials inducing MI was presented in Ref. [37], the interplay between relaxation of nonlinear response and coupling coefficient dispersion in the MI of dual core optical fiber [38], MI in an array of positive- and negative-index waveguides [39], MI in nonlinear positive-negative index couplers with saturable nonlinearity [40], MI of copropagating light beams induced by cubic-quintic nonlinearity in nonlinear negative-index material [41], MI in nonlinear oppositely directed coupler with a negative-index metamaterial channel [42], and so on. Furthermore, some systems can exhibit significant changes in the spectrum of the MI due to higher order effects [43–50]. To be specific, the influence of self-steepening and intrapulse Raman scattering on MI in oppositely directed coupler was studied [46].

Regarding to the effects of a nonlinear saturation present in some physical systems of interest, the band of instability may present significant changes in its amplitude and/or shape, and may even vanishing. This has motivated to investigate the MI in several saturable nonlinear systems such as waveguides [27, 51], optical fibers [36, 52], negative refractive metamaterial [53], metamaterials [50, 54, 55], optical fibers with higher-order dispersion [49, 56, 57], fibers with saturable delayed nonlinear response [58], positive-negative index couplers [40], semiconductor-doped glass fibers [26], and liquid-core photonic crystal fibers [59].

The aim of the present work is to investigate the influence of a saturable nonlinearity on the MI in oppositely directed coupler in the presence of high-order effects. As a particular case of our model, in the absence of saturation the system should present similar results to those obtained in [46] for the effects of self-steepening and intrapulse Raman scattering on the MI.

The paper is organized as follows: We introduce the theoretical model and present the analytical results for the power gain in the next section; in Sec. III we display the numerical results, in which we check the influence of self-steepening and intrapulse Raman scattering on the MI in Subsecs. III A and III B, respectively. Our conclusions are shown in Sec. IV.

## II. THEORETICAL MODEL

The model that describes the propagation of a high intense optical beam in oppositely directed coupler is given by the pair of linearly coupled nonlinear Schrödinger equations (CNLSE) with the form [36, 46]:

$$i\sigma_1 \frac{\partial u_1}{\partial z} - \frac{\beta_{21}}{2} \frac{\partial^2 u_1}{\partial x^2} + \kappa_{12} u_2 e^{-i\delta z} + \gamma_1 \{f(\Gamma|u_1|^2)u_1 + is_1 \frac{\partial(f(\Gamma|u_1|^2)u_1)}{\partial x} - T_{R1} u_1 \frac{\partial(f(\Gamma|u_1|^2))}{\partial x}\} = 0, \quad (1a)$$

$$i\sigma_2 \frac{\partial u_2}{\partial z} - \frac{\beta_{22}}{2} \frac{\partial^2 u_2}{\partial x^2} + \kappa_{21} u_1 e^{i\delta z} + \gamma_2 \{f(\Gamma|u_2|^2)u_2 + is_2 \frac{\partial(f(\Gamma|u_2|^2)u_2)}{\partial x} - T_{R2} u_2 \frac{\partial(f(\Gamma|u_2|^2))}{\partial x}\} = 0, \quad (1b)$$

where  $\sigma_1$  and  $\sigma_2$  indicate the sign of refractive index in channel-1 and channel-2 of the coupler, respectively. In order to compare the results obtained by our model with those presented in Ref. [46], we consider here the channel-1 made by positive index material and channel-2 by negative index material, hence  $\sigma_1 = 1$  and  $\sigma_2 = -1$ ;  $\beta_{21}$  and  $\beta_{22}$  are group velocity dispersion coefficients,  $u_1(z, x)$  and  $u_2(z, x)$  stand for the normalized complex amplitude of the modes in channels 1 and 2,  $\kappa_{12}$  and  $\kappa_{21}$  are linear coupling coefficients,  $\delta = \beta_1 - \beta_2$ , where  $\beta_1$  and  $\beta_2$  represent the propagation constants of the individual channels;  $\gamma_1$  and  $\gamma_2$  are the nonlinear coefficients related to self-phase modulation,  $s_1$  and  $s_2$  represent self-steepening effects, and  $T_{R1}$  and  $T_{R2}$  are responsible for the Raman-induced frequency shift, induced by intrapulse Raman scattering. Also, in this model we neglect the cross-phase modulation effects.

To be more specific, in the next steps, the functions  $f(\Gamma|u_1|^2)$  and  $f(\Gamma|u_2|^2)$  standing for the dependence of the refractive index with the intensity of the incident radiation will be described by a model widely used in the

literature describing the saturable nonlinearity as follows [56, 60, 61]

$$f(\Gamma|u_j|^2) = \frac{|u_j|^2}{1 + \Gamma|u_j|^2}, \quad (2)$$

where  $\Gamma = 1/P_s$  is the saturation parameter with  $P_s$  being the saturation power.

### A. Modulation instability

In order to verify the influence of a saturable nonlinearity on the MI we use the standard linear stability analysis. The basic idea of linear stability analysis is to perturb a continuous wave solution and then analyze whether this small perturbation grows or decays with propagation. For this, consider that the steady-state solutions of Eqs. (1a) and (1b) can be written as

$$u_1(z) = a_1 e^{iqz} e^{-i\frac{\delta}{2}z}, \quad (3a)$$

$$u_2(z) = a_2 e^{iqz} e^{i\frac{\delta}{2}z}, \quad (3b)$$

with  $a_j = \sqrt{P_j}$ , and  $P_j$  is the input power in the coupler  $j = 1, 2$ . By inserting the Eqs. (3a) and (3b) in Eqs. (1a) and (1b) one obtains the terms  $q$  and  $\delta$  given by

$$q = \frac{1}{2} \left[ \kappa_{12} h - \kappa_{21} h^{-1} + \frac{\gamma_1 R}{1 + \Gamma R} - \frac{\gamma_2 R h^2}{1 + \Gamma R h^2} \right], \quad (4a)$$

$$\delta = - \left[ \kappa_{21} h^{-1} + \kappa_{12} h + \frac{\gamma_1 R}{1 + \Gamma R} + \frac{\gamma_2 R h^2}{1 + \Gamma R h^2} \right], \quad (4b)$$

where  $h \equiv a_2/a_1$ , which describes how the total power  $P = a_1^2 + a_2^2$  is divided between forward and backward propagating waves, and  $R \equiv P/(1 + h^2)$ .

Next, we assume the steady-state solutions (3a) and (3b) can be perturbed by the functions  $\alpha_j(z, x)$ , such that

$$u_1(z, x) = [a_1 + \alpha_1(z, x)] e^{iqz} e^{-i\frac{\delta}{2}z}, \quad (5a)$$

$$u_2(z, x) = [a_2 + \alpha_2(z, x)] e^{iqz} e^{i\frac{\delta}{2}z}, \quad (5b)$$

where  $\alpha_i(z, x)$  is a small perturbation satisfying  $|\alpha_i(z, x)| \ll \sqrt{P_i}$ . Now, consider the perturbation terms as combinations of plane waves with the following form

$$\alpha_j(z, x) = c_j e^{i[Kz - \Omega x]} + d_j e^{-i[Kz - \Omega x]}, \quad (6)$$

where  $K$  and  $\Omega$  are wave-vector and frequency of perturbation amplitude. Thus, inserting the Eqs.(5a) and

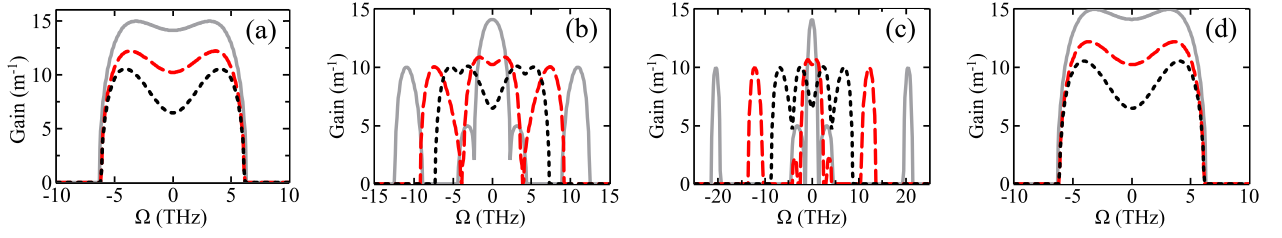


Figure 1. (Color online) Instability gain spectra in normal group velocity dispersion regime as function of saturation parameter under different combinations of  $s_1$  and  $s_2$  when  $P = 10\text{kW}$ ,  $\gamma_1 = \gamma_2 = 1/(\text{kW m})$ , and  $\kappa_{12} = \kappa_{21} = 10\text{m}^{-1}$  with (a)  $s_1 = s_2 = 0$ , (b)  $s_1 = 0$  and  $s_2 = 1\text{ ps}/(\text{kW m})$ , (c)  $s_1 = s_2 = 1\text{ ps}/(\text{kW m})$ , and (d)  $s_1 = -s_2 = 1\text{ ps}/(\text{kW m})$ . The saturation parameter values used herein are:  $\Gamma = 0$  in solid-line (gray),  $\Gamma = 0.1\text{ kW}^{-1}$  in dashed-line (red), and  $\Gamma = 0.4\text{ kW}^{-1}$  in dotted-line (black). The other parameters are  $T_{R1} = T_{R2} = 0\text{ ps}/(\text{kW m})$ ,  $h = 1$  and  $\beta_{21} = \beta_{22} = 1\text{ ps}^2\text{ m}^{-1}$ .

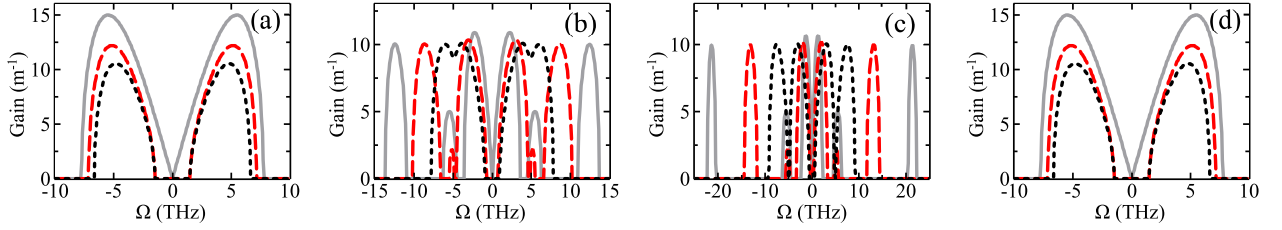


Figure 2. (Color online) Instability gain spectra in anomalous group velocity dispersion regime as function of saturation parameter under different combinations of  $s_1$  and  $s_2$  when  $P = 10\text{kW}$ ,  $\gamma_1 = \gamma_2 = 1/(\text{kW m})$ , and  $\kappa_{12} = \kappa_{21} = 10\text{m}^{-1}$  with (a)  $s_1 = s_2 = 0$ , (b)  $s_1 = 0$  and  $s_2 = 1\text{ ps}/(\text{kW m})$ , (c)  $s_1 = s_2 = 1\text{ ps}/(\text{kW m})$ , and (d)  $s_1 = -s_2 = 1\text{ ps}/(\text{kW m})$ . The saturation parameter values used herein are:  $\Gamma = 0$  in solid-line (gray),  $\Gamma = 0.1\text{ kW}^{-1}$  in dashed-line (red), and  $\Gamma = 0.4\text{ kW}^{-1}$  in dotted-line (black). The other parameters are  $T_{R1} = T_{R2} = 0\text{ ps}/(\text{kW m})$ ,  $h = -1$  and  $\beta_{21} = \beta_{22} = -1\text{ ps}^2\text{ m}^{-1}$ .

(5b) in (1a) and (1b), after some mathematical manipulations, one obtains the linearized equations

$$i\frac{\partial\alpha_1}{\partial z} - \frac{\beta_{21}}{2}\frac{\partial^2\alpha_1}{\partial x^2} + \frac{\gamma_1 R}{(1+\Gamma R)^2} [\alpha_1(1+\Gamma R) + \alpha_1^*] - \alpha_1\kappa_{12}h + \alpha_2\kappa_{12} + \frac{i\gamma_1 s_1 R}{(1+\Gamma R)^2} \left[ \frac{\partial\alpha_1}{\partial x} (2+\Gamma R) \right] - \frac{\gamma_1 T_{R1} R}{(1+\Gamma^2+2\Gamma R)} \frac{\partial\alpha_1}{\partial x} = 0, \quad (7a)$$

$$-i\frac{\partial\alpha_2}{\partial z} - \frac{\beta_{22}}{2}\frac{\partial^2\alpha_2}{\partial x^2} + \frac{\gamma_2 R h^2}{(1+\Gamma R h^2)^2} [\alpha_2(1+\Gamma R h^2) + \alpha_2^*] - \alpha_2\kappa_{21}h^{-1} + \alpha_1\kappa_{21} + \frac{i\gamma_2 s_2 R h^2}{(1+\Gamma R h^2)^2} \left[ \frac{\partial\alpha_2}{\partial x} (2+\Gamma R h^2) \right] - \frac{\gamma_2 T_{R2} R h^2}{(1+\Gamma^2+2\Gamma R h^2)} \frac{\partial\alpha_2}{\partial x} = 0. \quad (7b)$$

Substituting Eq. (6) into Eqs. (7a) and (7b), one gets a set of four linearly coupled equations satisfied by  $c_j$  and  $d_j$ . This set of coupled equations can be written in matrix form

$$\begin{pmatrix} m_{11} & m_{12} & m_{13} & m_{14} \\ m_{21} & m_{22} & m_{23} & m_{24} \\ m_{31} & m_{32} & m_{33} & m_{34} \\ m_{41} & m_{42} & m_{43} & m_{44} \end{pmatrix} \begin{pmatrix} c_1 \\ c_2 \\ d_1 \\ d_2 \end{pmatrix} = 0,$$

where the matrix elements are given by:  $m_{11} = 0$ ;  $m_{12} = \frac{\gamma_2 R h^2}{(1+\Gamma R h^2)^2}$ ;  $m_{13} = \kappa_{21}$ ;  $m_{14} = -K + \frac{\beta_{22}}{2}\Omega^2 - \kappa_{21}h^{-1} + \frac{\gamma_2 R h^2}{(1+\Gamma R h^2)} - \frac{\gamma_2 s_2 R h^2 \Omega (2+\Gamma R h^2)}{(1+\Gamma R h^2)^2} - \frac{i\gamma_2 T_{R2} R h^2 \Omega}{(1+\Gamma^2+2\Gamma R h^2)}$ ;  $m_{21} = \frac{\gamma_1 R}{(1+\Gamma R)^2}$ ;  $m_{22} = 0$ ;  $m_{23} = K + \frac{\beta_{21}}{2}\Omega^2 - \kappa_{12}h + \frac{\gamma_1 R}{(1+\Gamma R)} - \frac{\gamma_1 s_1 R \Omega (2+\Gamma R)}{(1+\Gamma R)^2} - \frac{i\gamma_1 T_{R1} R \Omega}{(1+\Gamma^2+2\Gamma R)}$ ;  $m_{24} = \kappa_{12}$ ;  $m_{31} = \kappa_{21}$ ;  $m_{32} = K + \frac{\beta_{22}}{2}\Omega^2 - \kappa_{21}h^{-1} + \frac{\gamma_2 R h^2}{(1+\Gamma R h^2)} + \frac{\gamma_2 s_2 R h^2 \Omega (2+\Gamma R h^2)}{(1+\Gamma R h^2)^2} + \frac{i\gamma_2 T_{R2} R h^2 \Omega}{(1+\Gamma^2+2\Gamma R h^2)}$ ;  $m_{33} = 0$ ;  $m_{34} = \frac{\gamma_2 R h^2}{(1+\Gamma R h^2)^2}$ ;  $m_{41} = -K + \frac{\beta_{21}}{2}\Omega^2 - \kappa_{12}h + \frac{\gamma_1 R}{(1+\Gamma R)} + \frac{\gamma_1 s_1 R \Omega (2+\Gamma R)}{(1+\Gamma R)^2} + \frac{i\gamma_1 T_{R1} R \Omega}{(1+\Gamma^2+2\Gamma R)}$ ;  $m_{42} = \kappa_{12}$ ;  $m_{43} = \frac{\gamma_1 R}{(1+\Gamma R)^2}$ ; and  $m_{44} = 0$ .

The determinant of the matrix  $M$  leads to a fourth order polynomial in  $K$ , where the roots should possess a nonzero and negative imaginary part that corresponds to a dispersion relation. MI occurs when the wave number possesses a nonzero imaginary part leading to an exponential growth of the perturbed amplitude. The MI is measured by power gain, and it is defined at any pump frequency as [40]

$$G(\Omega) \equiv |\Im \{K_{\max}\}|, \quad (8)$$

where  $\Im \{K_{\max}\}$  denotes the imaginary part of the root with the largest value  $K_{\max}(\Omega)$ .

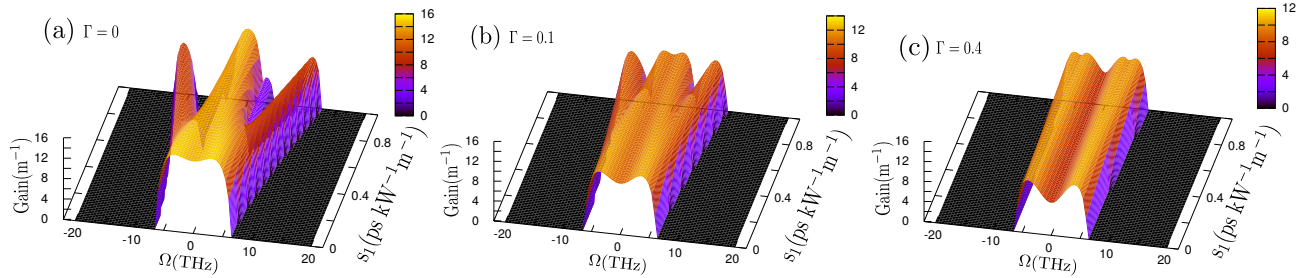


Figure 3. (Color online) Instability gain spectra showing the influence of the self-steepening effect in channel 1 ( $s_2 = 0$ ) in normal group velocity dispersion regime for different values of saturation parameter. The other parameters are the same ones used in Fig. 1.

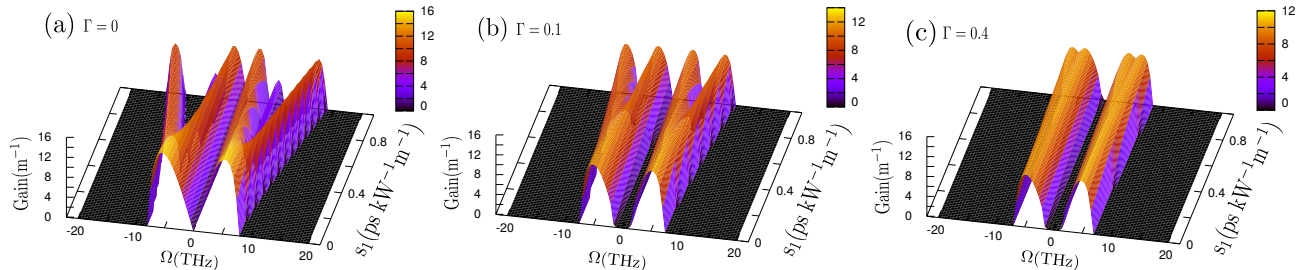


Figure 4. (Color online) Instability gain spectra showing the influence of the self-steepening effect in channel 1 ( $s_2 = 0$ ) in anomalous group velocity dispersion regime for different values of saturation parameter. The other parameters are the same ones used in Fig. 2.

### III. NUMERICAL RESULTS

#### A. Effect of self-steepening on modulation instability

Firstly we focus on the influence of self-steepening effect on MI in oppositely directed coupler for different values of saturation parameter. To this end, we omit the Raman self-scattering effect by setting  $T_{R1} = T_{R2} = 0$ . In Fig. 1 we consider MI in normal group velocity in dispersion regime under different combinations of  $s_1$  and  $s_2$ , considering  $h = 1$  and  $\beta_{21} = \beta_{22} = 1 \text{ ps}^2 \text{ m}^{-1}$ , for simplicity. Also, the MI for the anomalous case of group velocity dispersion is illustrated in Fig. 2, where we have used  $h = -1$  and  $\beta_{21} = \beta_{22} = -1 \text{ ps}^2 \text{ m}^{-1}$ . The other parameters that we used were  $\kappa_{12} = \kappa_{21} = 10 \text{ m}^{-1}$ ,  $\gamma_1 = \gamma_2 = 1 / (\text{kW m})$ , and  $P = 10 \text{ kW}$ .

*Normal group velocity dispersion* - To be more specific, in Fig. 1(a) we display the case without self-steepening effects ( $s_1 = s_2 = 0$ ) for three different values of saturation parameter:  $\Gamma = 0$  in solid-line (gray),  $\Gamma = 0.1 \text{ kW}^{-1}$  in dashed-line (red), and  $\Gamma = 0.4 \text{ kW}^{-1}$  in dotted-line (black). These parameters are also used in Figs. 1(b)-(d). Note in Fig. 1(a) that the instability spectra consists of single conventional MI band centered at zero perturbation frequency formed by balance between group velocity dispersion and self-phase modulation. However, when increasing the value of the saturation parameter the instability gain decreases faster for frequencies near

to  $\Omega = 0$ . We stress that in the present model, for the normal group velocity dispersion regime, the instability gain exists even if perturbation frequency is zero [46].

In Fig. 1(b) we study the self-steepening effect in only one of the channels by tuning  $s_1 = 0$  and  $s_2 = 1 \text{ ps} / (\text{kW m})$ . In this figure is evident the influence of the value of the saturation parameter on the number of MI bands. The greater the value of this parameter is, more centralized will be the gain region, thereby decreasing the amount of MI bands. The results for the two channels with the self-steepening effect are shown in Fig. 1(c), where we have used  $s_1 = s_2 = 1 \text{ ps} / (\text{kW m})$ . Note that without saturation ( $\Gamma = 0$ ) there are two MI bands centered close to  $\Omega = \pm 20 \text{ THz}$  plus three close to  $\Omega = 0$ . By increasing the saturation parameter for  $\Gamma = 0.1 \text{ kW}^{-1}$  we observe only three bands centered close to  $\Omega = 0$ . And, when setting  $\Gamma = 0.4 \text{ kW}^{-1}$  we see the appearance of only one MI band. This is also evident when one looks at Fig. 3, where we show a 3D surface of the instability gain as a function of the perturbation frequency and self-steepening parameter  $s_1$ , for three different values of the saturation parameter, i.e.,  $\Gamma = 0$  in Fig. 3(a),  $\Gamma = 0.1 \text{ kW}^{-1}$  in Fig. 3(b), and  $\Gamma = 0.4 \text{ kW}^{-1}$  in Fig. 3(c).

Fig. 1(d) displays the case in which both channels are influenced by self-steepening effect but opposite in sign (here we set  $s_1 = -s_2 = 1 \text{ ps} / (\text{kW m})$ ). Note that, in Fig. 1(d), as well as shown in Ref. [46] for the case with-



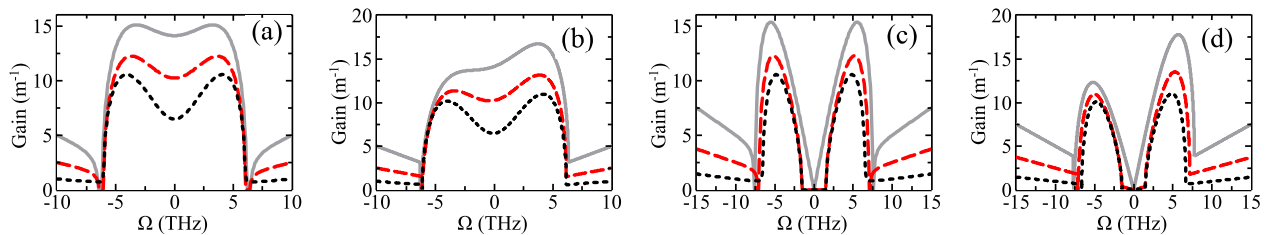


Figure 5. (Color online) Instability gain spectra showing the effect of intrapulse Raman scattering in normal group velocity dispersion regime ( $h = 1$  and  $\beta_{21} = \beta_{22} = 1 \text{ ps}^2 \text{ m}^{-1}$ ) for (a)  $T_{R1} = T_{R2} = 0.1 \text{ ps}/(\text{kW m})$  and (b)  $T_{R1} = -T_{R2} = 0.1 \text{ ps}/(\text{kW m})$  and in anomalous group velocity dispersion regime ( $h = -1$  and  $\beta_{21} = \beta_{22} = -1 \text{ ps}^2 \text{ m}^{-1}$ ) for (c)  $T_{R1} = T_{R2} = 0.1 \text{ ps}/(\text{kW m})$  and (d)  $T_{R1} = -T_{R2} = 0.1 \text{ ps}/(\text{kW m})$ . The other parameters are  $P = 10 \text{ kW}$ ,  $\gamma_1 = \gamma_2 = 1/(\text{kW m})$ ,  $\kappa_{12} = \kappa_{21} = 10 \text{ m}^{-1}$ , and  $s_1 = s_2 = 0$ . The saturation parameter values used herein are:  $\Gamma = 0$  in solid-line (gray),  $\Gamma = 0.1 \text{ kW}^{-1}$  in dashed-line (red), and  $\Gamma = 0.4 \text{ kW}^{-1}$  in dotted-line (black).

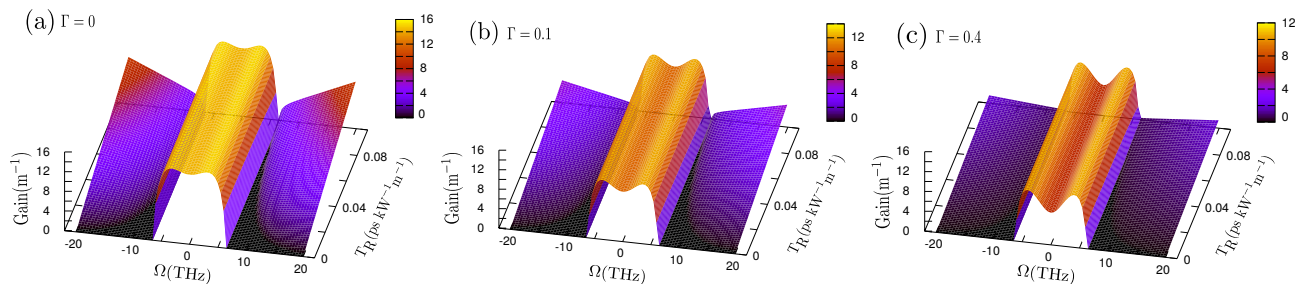


Figure 6. (Color online) Instability gain spectra versus the effect of intrapulse Raman scattering (with  $T_{R1} = T_{R2} = T_R$ ) in normal group velocity dispersion regime for different values of saturation parameter. The other parameters are the same ones used in Fig. 5(a).

out saturation, the gain presents a similar behavior to the case where both channels are not influenced by self-steepening effect (Fig. 1(a)). Indeed, we have observed that the effective influence of self-steepening parameters depends on its algebraic sum, i.e., this effect is canceled in the gain shown by Fig. 1(d). This can be checked by comparing the dashed or dotted-lines of Figs. 1(a) and 1(d).

*Anomalous group velocity dispersion* - Differently from the normal dispersion, in the anomalous case there is no instability gain at zero perturbation frequency. Also, as previously verified [46], one can see in Fig. 2 that the maximum gain and the band width are influenced by the presence of self-steepening effect. However, when saturation is present one can verify a gain reduction and a separation of the bands. This is evident when one look at the 3D surfaces of the instability gain for different values of the saturation parameter:  $\Gamma = 0$  in Fig. 4(a),  $\Gamma = 0.1 \text{ kW}^{-1}$  in Fig. 4(b), and  $\Gamma = 0.4 \text{ kW}^{-1}$  in Fig. 4(c).

In Fig. 2(a) we display the case without self-steepening effects ( $s_1 = s_2 = 0$ ) for three different values of saturation parameter:  $\Gamma = 0$  in solid-line (gray),  $\Gamma = 0.1 \text{ kW}^{-1}$  in dashed-line (red), and  $\Gamma = 0.4 \text{ kW}^{-1}$  in dotted-line (black). Note the differences we just mentioned comparing the Fig. 2(a) with Fig. 1(a). Also, differently from the single null point that we obtain at

$\Omega = 0$  for the case without saturation, in the presence of saturation we observe a large hole in the gain region near  $\Omega = 0$ .

In Fig. 2(b) we show the self-steepening effect in only one of the channels by tuning  $s_1 = 0$  and  $s_2 = 1 \text{ ps}/(\text{kW m})$ . By increasing the value of the saturation parameter we observe a compactification of instability bands, a result similar to that obtained for normal dispersion, but now with null gain for disturbance near zero. This can also be seen in Fig. 2(c), in which we consider two channels with the self-steepening effect (by adjusting  $s_1 = s_2 = 1 \text{ ps}/(\text{kW m})$ ).

The case in which both channels are influenced by self-steepening effect but opposite in sign (considered in Fig. 2(d) for  $s_1 = -s_2 = 1 \text{ ps}/(\text{kW m})$ ) shows the same behavior when compared to the case without self-steepening effects (Fig. 2(a)).

## B. Effect of intrapulse Raman scattering on modulation instability

Next, we study the effect of intrapulse Raman scattering on MI in oppositely directed couplers as a function of saturation parameter. For this particular study, we neglect the role of self-steepening effect (by setting

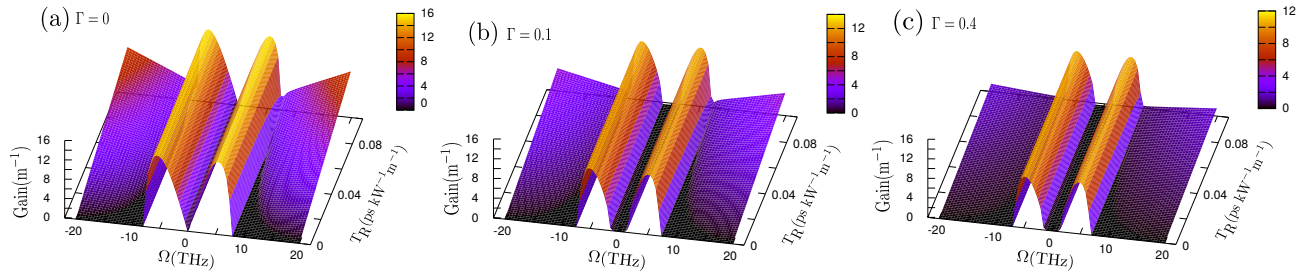


Figure 7. (Color online) Instability gain spectra versus the effect of intrapulse Raman scattering (with  $T_{R1} = T_{R2} = T_R$ ) in anomalous group velocity dispersion regime for different values of saturation parameter. The other parameters are the same ones used in Fig. 5(c).

$s_1 = s_2 = 0$ ). Here, we use the same parameters used in the previous subsection, i.e.,  $\kappa_{12} = \kappa_{21} = 10 \text{ m}^{-1}$ ,  $\gamma_1 = \gamma_2 = 1/(\text{kW m})$ , and  $P = 10 \text{ kW}$ .

In Figs. 5(a) and 5(b) we consider MI in normal group velocity in dispersion regime under an intrapulse Raman scattering effect with amplitude  $T_{R1} = T_{R2} = 0.1 \text{ ps}/(\text{kW m})$  and  $T_{R1} = -T_{R2} = 0.1 \text{ ps}/(\text{kW m})$ , respectively, and considering  $h = 1$  and  $\beta_{21} = \beta_{22} = 1 \text{ ps}^2 \text{ m}^{-1}$ , for simplicity. Also, the MI for the anomalous case of group velocity dispersion is illustrated in Figs. 5(c) and 5(d), where we have  $T_{R1} = T_{R2} = 0.1 \text{ ps}/(\text{kW m})$  and  $T_{R1} = -T_{R2} = 0.1 \text{ ps}/(\text{kW m})$ , respectively, plus  $h = -1$  and  $\beta_{21} = \beta_{22} = -1 \text{ ps}^2 \text{ m}^{-1}$ . The solid-lines (gray) in Figs. 5(a)-(d) represent the cases without saturation effect ( $\Gamma = 0$ ) while in the dashed-lines (red) and dotted-lines (black) we analyzed the effects of the saturation characterized by the parameters  $\Gamma = 0.1 \text{ kW}^{-1}$  and  $\Gamma = 0.4 \text{ kW}^{-1}$ , respectively. Note that in the absence of intrapulse Raman scattering, one retrieves the results shown in Figs. 1(a) and 2(a) for the cases of normal and anomalous dispersion, respectively. Then, by comparing the Figs. 5(a)-(d) with Figs. 1(a) and 2(a) one observes the appearance of a tail for highest perturbation frequencies that makes de instability gain to increase linearly in these regions. However, by increasing the saturation effect the maximum in these instability gain are reduced also in its tails (see dashed-lines and dotted lines in Fig. 5). Also, differently from the cases shown in Figs. 5(a) and 5(c), when the Raman scattering coefficients are opposite in sign there will be a symmetry breaking in the gain regions (Figs. 5(b) and 5(d)).

Finally, by increasing the Raman scattering intrapulse will cause a linear increase in the maximum MI in the tail regions while maintaining the core bands largely unchanged. This can be visualized in the 3D surfaces shown in Figs. 6 and 7 for the cases of normal and anomalous dispersion, respectively, with  $T_{R1} = T_{R2} = T_R$  and for three values of the saturation parameter.

#### IV. CONCLUSION

To summarize we have studied the modulation instability in oppositely directed coupler with higher-order effects and saturable nonlinearities for both normal and anomalous group velocity dispersion regimes. It is found that the instability bands under saturation effects, besides reducing its amplitude, it also makes the bands gathered together around the zero perturbation frequency when the system presents self-steepening effects. However, in anomalous group velocity dispersion regime this compactification due to the growth of the saturation parameter is followed by an increase in the null gain region near  $\Omega = 0$ , enlarging the separation of the instability bands close to this point.

In the case of intrapulse Raman scattering, new instability regions are created in the tail of the original MI bands (by original bands we emphasize the case without this effect). In this case the saturation effects causes a change in the center of the gain region decreasing the width of the bands, followed by an attenuation in the amplitude of the instability gain. Also, the symmetry shown in the MI regions, when the Raman scattering coefficients are equal in sign, are broken for Raman scattering coefficients opposite in sign. Finally, the present study reinforces those results presented in Ref. [46] providing a new way to generate solitons or ultrashort pulses in oppositely directed coupler with saturable nonlinearities.

We thank the Brazilian agencies CNPq, CAPES, FAPEG, and Instituto Nacional de Ciência e Tecnologia-Informática Quântica (INCT-IQ) for partial support.

- 
- [1] A. Hasegawa, Phys. Rev. A 1, 1746 (1970).
  - [2] C. J. McKinstrie and R. Bingham, Phys. Fluids B 4, 2626 (1992).
  - [3] P. Sprangle, J. Krall, and E. Esarey, Phys. Rev. Lett. 73, 3544 (1994).
  - [4] S. Guérin, G. Laval, P. Mora, J. C. Adam, A. Héron, and A. Bendib, Phys. Plasmas 2, 2807 (1995).

- [5] E. Mjølhus, *J. Plasma Physics* 16, 321 (1976).
- [6] K. Tai, A. Hasegawa, and A. Tomita, *Phys. Rev. Lett.* 56, 135 (1986).
- [7] G. P. Agrawal, *Phys. Rev. Lett.* 59, 880 (1987).
- [8] M. R. Amin, G. E. Morfill, and P. K. Shukla, *Phys. Rev. E* 58, 6517 (1998).
- [9] D. Kip, M. Soljačić, M. Segev, E. Eugenieva, and D. N. Christodoulides, *Science* 290, 495 (2000).
- [10] M. Soljačić, M. Segev, T. Coskun, D. N. Christodoulides, and A. Vishwanath, *Phys. Rev. Lett.* 84, 467 (2000).
- [11] V. V. Konotop and M. Salerno, *Phys. Rev. A* 65, 021602(R) (2002).
- [12] L. Salasnich, A. Parola, and L. Reatto, *Phys. Rev. Lett.* 91, 080405 (2003).
- [13] L. D. Carr and J. Brand, *Phys. Rev. Lett.* 92, 040401 (2004).
- [14] L. Li, Z. Li, B. A. Malomed, D. Mihalache, and W. M. Liu, *Phys. Rev. A* 72, 033611 (2005).
- [15] M. Peccianti, C. Conti, G. Assanto, A. De Luca, and C. Umeton, *Nature* 432, 733 (2004).
- [16] M. Onorato, A. R. Osborne, and M. Serio, *Phys. Rev. Lett.* 96, 014503 (2006).
- [17] M. Onorato *et al.*, *Phys. Rev. Lett.* 102, 114502 (2009).
- [18] M. Karlsson, *J. Opt. Soc. Am. B* 12, 2071 (1995).
- [19] P. St. J. Russell and J.-L. Archambault, *J. Phys. III France* 4, 2471 (1994).
- [20] S. Trillo and P. Ferro, *Opt. Lett.* 20, 438 (1995).
- [21] U. Streppel, D. Michaelis, R. Kowarschik, and A. Braüer, *Phys. Rev. Lett.* 95, 073901 (2005).
- [22] W. Królikowski, O. Bang, J. J. Rasmussen, and J. Wyller, *Phys. Rev. E* 64, 016612 (2001).
- [23] R. Schiek, H. Fang, R. Malendevich, and G. I. Stegeman, *Phys. Rev. Lett.* 86, 4528 (2001).
- [24] H. P. Wong, *Opt. Commun.* 213, 173 (2002).
- [25] F. Kh. Abdullaev, S. A. Darmanyany, S. Bischoff, and M. P. Sorensen, *J. Opt. Soc. Am. B* 14, 27 (1997).
- [26] J. M. Hickmann, S. B. Cavalcanti, N. M. Borges, E. A. Gouveia, and A. S. Gouveia-Neto, *Opt. Lett.* 18, 182 (1993).
- [27] N. Da Dalt, C. De Angelis, G. F. Nalesso, and M. Santagiustina, *Opt. Commun.* 121, 69 (1995).
- [28] A. Hasegawa, *Opt. Lett.* 9, 288 (1984).
- [29] K. Tai, A. Tomita, J. L. Jewell, and A. Hasegawa, *Appl. Phys. Lett.* 49, 236 (1986).
- [30] V. E. Zakharova and L. A. Ostrovsky, *Physica D* 238, 540 (2009).
- [31] S. Trillo, S. Wabnitz, G. I. Stegeman, and E. M. Wright, *J. Opt. Soc. Am. B* 6, 889 (1989).
- [32] J. Meier, D. N. Christodoulides, G. I. Stegeman, H. Yang, G. Salamo, R. Morandotti, J. S. Aitchison, and Y. Silberberg, *Opto-Electron. Rev.* 13, 75 (2005).
- [33] J. H. Li, K. S. Chiang, and K. W. Chow, *J. Opt. Soc. Am. B* 28, 1693 (2011).
- [34] J. H. Li, K. S. Chiang, B. A. Malomed, and K. W. Chow, *J. Phys. B: At. Mol. Opt. Phys.* 45, 165404 (2012).
- [35] W. Ding *et al.*, *Opt. Lett.* 37, 668 (2012).
- [36] K. Nithyanandan, R. V. J. Raja, and K. Porsezian, *Phys. Rev. A* 87, 043805 (2013).
- [37] K. Ogusu and H. Li, *J. Lightwave Technol.* 31, 2639 (2013).
- [38] K. Nithyanandan and K. Porsezian, *Opt. Commun.* 303, 46 (2013).
- [39] L. Zhang, Y. Xiang, X. Dai, and S. Wen, *J. Opt. Soc. Am. B* 31, 3029 (2014).
- [40] P. H. Tatsing, A. Mohamadou, C. Bouri, C. G. L. Tiofack, and T. C. Kofane, *J. Opt. Soc. Am. B* 29, 3218 (2012).
- [41] R. Gupta, T. S. Raju, C. N. Kumar, and P. K. Panigrahi, *J. Opt. Soc. Am. B* 29, 3360 (2012).
- [42] Y. Xiang, S. Wen, X. Dai, and D. Fan, *Phys. Rev. E* 82, 056605 (2010).
- [43] R. Ganapathy and V. C. Kuriakose, *Pramana-J. Phys.* 58, 669 (2002).
- [44] K. Nithyanandan, R. V. J. Raja, K. Porsezian, and B. Kalithasan, *Phys. Rev. A* 86, 023827 (2012).
- [45] T. Hu and X. Sun, *Laser Phys. Lett.* 10, 095101 (2013).
- [46] A. K. Shafeeque Ali, K. Porsezian, and T. Uthayakumar, *Phys. Rev. E* 90, 042910 (2014).
- [47] A. Mohamadou, P. H. Tatsing, C. G. Latchio Tiofack, C. B. Tabi, and T. C. Kofane, *J. Mod. Optic* 61, 1670 (2014).
- [48] A. S. Reyna and C. B. de Araujo, *Phys. Rev. A* 89, 063803 (2014).
- [49] K. Nithyanandan, R. V. J. Raja, T. Uthayakumar, and K. Porsezian, *Pramana-J. Phys.* 82, 339 (2014).
- [50] X. Zhong and K. Cheng, *Optik* 125, 6733 (2014).
- [51] M. Stepic, C. E. Rüter, D. Kip, A. Maluckov, and L. Hadžievski, *Opt. Commun.* 267, 229 (2006).
- [52] M. L. Lyra and A. S. Gouveia-Neto, *Opt. Commun.* 108, 117 (1994).
- [53] X. Zhong, T. Tang, A. Xiang, and K. Cheng, *Opt. Commun.* 284, 4727 (2011).
- [54] Y. Xiang, X. Dai, S. Wen, and D. Fan, *J. Opt. Soc. Am. B* 28, 908 (2011).
- [55] X. Zhong, K. Cheng, and K. S. Chiang, *J. Opt. Soc. Am. B* 31, 1484 (2014).
- [56] P. T. Dinda and K. Porsezian, *J. Opt. Soc. Am. B* 27, 1143 (2010).
- [57] K. Porsezian, K. Nithyanandan, R. V. J. Raja, and P. K. Shukla, *J. Opt. Soc. Am. B* 29, 2803 (2012).
- [58] G. L. da Silva, I. Gleria, M. L. Lyra, and A. S. B. Sombra, *J. Opt. Soc. Am. B* 26, 183 (2009).
- [59] R. V. J. Raja, K. Porsezian, and K. Nithyanandan, *Phys. Rev. A* 82, 013825 (2010).
- [60] Y.-F. Chen, K. Beckwitt, F. W. Wise, B. G. Aitken, J. S. Sanghera, and I. D. Aggarwal, *J. Opt. Soc. Am. B* 23, 347 (2006).
- [61] S. Gatz and J. Herrmann, *J. Opt. Soc. Am. B* 8, 2296 (1991).